

Determining the physical limits on semi-active control performance: A tutorial

P. S. Harvey Jr., H. P. Gavin, J. T. Scruggs and J. M. Rinker

February 6, 2013

Abstract

Control forces in semi-active control systems are constrained by the dynamics of actuators that regulate energy transmission through variable damping and/or stiffness mechanisms. The potential benefit of developing and implementing new semi-active control devices and applications can be determined by optimizing the controlled performance subject to the constraints of the dynamics of the system being controlled (given by the state equations), the constraints associated with the dynamics of the semi-active device, and the expected external forcing.

Performance optimization of semi-active control systems is a constrained two-point boundary value problem. This paper shows how this constrained problem can be transformed into an unconstrained problem and how to easily solve the related unconstrained problem with `MATLAB`. The method is illustrated on the performance optimization of a simple semi-active tuned-mass-damper for a structure subjected to ground accelerations. Several possible extensions of this method and application are described in detail.

1 Introduction

Over the last several decades a large number of semi-active control devices have been developed for a broad range of applications. Since the publication of review articles on semi-active control [1, 2], research has progressed on semi-active stiffness devices [3, 4, 5, 6, 7], semi-active damping devices [8, 9, 10], and semi-active friction devices [11, 12]. Models for these devices involve constraints, either directly on device forces, or indirectly on an internal variable such as a valve position, a solenoid voltage, or an electrical resistance.

There are two principle advantages of implementing semi-active control. The first is that the power a semi-active device may regulate within the structure can be orders of magnitude greater than the power required to regulate the device properties (e.g., damping and/or stiffness). The second is that the controlled system is unconditionally stable in a bounded-input, bounded-output sense *regardless* of the feedback law implemented. A potential disadvantage of semi-active control systems is that, for some applications, closed-loop semi-active performance may be only marginally better than that of simpler passive control systems [1]. Additionally, actuation constraints of semi-active control systems render the system non-linear and performance can be assessed and optimized only through transient response simulations. It is common practice to evaluate the performance of semi-actively controlled systems for a particular feedback law and compare the result to a passively controlled system. This method of performance evaluation is insufficient as the performance of a semi-active device may vary greatly depending on the choice of the objective function and the feedback law.

To fully evaluate the potential benefit of a semi-active controls system it is essential to examine its optimal performance. Methods of trajectory optimization for a particular objective function may be used to determine the *best possible performance* achievable within the constraints of a particular semi-active device, the structural system into which it is applied, and the external forcing. This optimization allows the proper performance evaluation of a new semi-active device and a meaningful method of comparison with existing semi-active devices and passive devices. Semi-active devices that can achieve performance levels sufficiently better than those of existing passive devices or alternative semi-active devices merit the development of control hardware and feedback control rules.

The correct formulation, and importance, of constrained control problems have been known for decades. Kirk emphasizes that “the optimal [constrained] control history ... *cannot* be determined, in general, by calculating the optimal [unconstrained] control history and allowing it to saturate whenever the stipulated boundaries are violated.” [13] (p. 236). Further, Tseng and Hedrick prove that “clipped-optimal is sub-optimal in the sense that it minimizes only the instantaneous performance index difference [and] does not guarantee optimality in minimizing [an integral] performance index.” [14] (p. 556).

We note here that in a dynamical control system, $\dot{\mathbf{x}} = \mathbf{f}(\mathbf{x}, \mathbf{u}; t)$, changing the controls \mathbf{u} at time t changes $\dot{\mathbf{x}}$ (but not \mathbf{x}) at time t . So any state-dependent performance index can not be instantaneously improved by changing the controls at time t . It is therefore rational to minimize integral cost functions. The choice of the objective function is subjective, and reflects the control engineer’s best judgment regarding the purpose of the control system.

Following the work of Tseng and Hedrick [14], this short paper states the semi-active control optimization problem as a constrained two-point boundary value problem (TPBVP), and gives a solution procedure by which the constraints are eliminated, reducing the problem to an unconstrained TPBVP. The method is illustrated on a simplified tuned-mass-damper (TMD) with an additional semi-active damper, in which the dynamics are linear (except for the actuation constraints) and the Lagrangian of the cost function is quadratic. The purpose of this paper is to provide a concise tutorial on semi-active performance optimization that illustrates, in detail, just how easy it is to setup and solve such problems.

2 Problem Statement

An admissible scalar control trajectory $u(t)$ is to be applied to a non-autonomous system

$$\dot{\mathbf{x}}(t) = \mathbf{A}\mathbf{x}(t) + \mathbf{B}u(t) + \mathbf{B}_w w(t), \quad \mathbf{x}(0) = \mathbf{x}_0, \quad \mathbf{x}(t) \in \mathbb{R}^n \quad (1)$$

in order to minimize the following cost functional of the states $\mathbf{x}(t)$ and control input $u(t)$:

$$J = \int_0^{t_f} L(\mathbf{x}, \mathbf{u}; t) dt \equiv \int_0^{t_f} \frac{1}{2} \begin{bmatrix} \mathbf{x}(t) \\ u(t) \end{bmatrix}' \begin{bmatrix} \mathbf{Q} & \mathbf{S} \\ \mathbf{S}' & R \end{bmatrix} \begin{bmatrix} \mathbf{x}(t) \\ u(t) \end{bmatrix} dt. \quad (2)$$

The linear, time-invariant plant (1) is parameterized as follows: $\mathbf{A} \in \mathbb{R}^{n \times n}$ is the dynamics matrix, $\mathbf{B} \in \mathbb{R}^n$ is the control input matrix, and $\mathbf{B}_w \in \mathbb{R}^n$ is the input matrix associated with the known, deterministic exogenous disturbance $w(t)$. The Lagrangian $L(\cdot)$ is quadratic with state weighting matrix $\mathbf{Q} \in \mathbb{R}^{n \times n}$, control weighting scalar R , and bilinear state-control weighting matrix $\mathbf{S} \in \mathbb{R}^n$.

Typically, controllable dampers have the performance limitations described by a maximum achievable control force amplitude u_{\max} and a maximum achievable damping coefficient c_{\max} . So, for semi-active damping, feasible control forces are bounded by sectors shown in Figure 1, where $v(t)$ is the velocity across the actuator. The former limitation implies $|u(t)| < u_{\max}$ and the latter implies

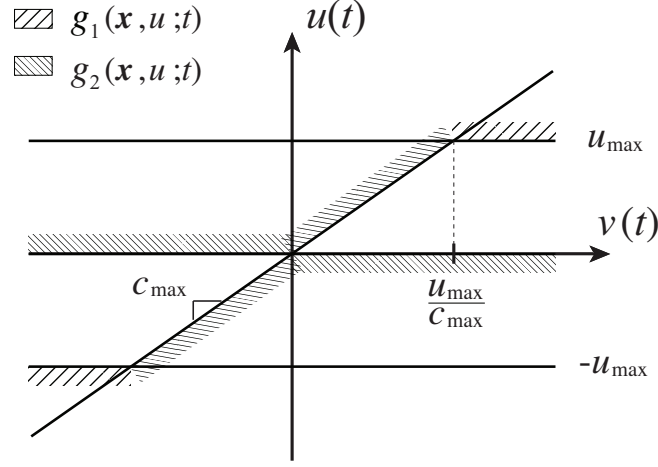


Figure 1: Sector-bound constraint for semi-active damping device. $v(t)$ is the velocity across the actuator.

$|u(t)| \in [0, c_{\max}|v(t)|]$; such constraints may be expressed by the following non-linear inequality constraint equations:

$$\mathbf{g}(\mathbf{x}, u; t) = \begin{bmatrix} u^2(t) - u_{\max}^2 \\ u(t)(u(t) - c_{\max}\mathbf{T}'\mathbf{x}(t)) \end{bmatrix} \leq \mathbf{0} \quad (3)$$

where the transformation vector $\mathbf{T} \in \mathbb{R}^n$ extracts the velocity across the actuator, $v(t) = \mathbf{T}'\mathbf{x}(t)$. For other semi-active device models, the feasible region may take other forms, as described in Section 5.

The minimization of J is subject to the equality constraint (1) and the inequality constraint (3). The Hamiltonian is therefore defined as

$$H(\mathbf{x}, \mathbf{u}, \mathbf{p}, \boldsymbol{\lambda}; t) \equiv L(\mathbf{x}, \mathbf{u}; t) + \mathbf{p}'(t)(\mathbf{A}\mathbf{x}(t) + \mathbf{B}\mathbf{u}(t) + \mathbf{B}_w w(t)) + \boldsymbol{\lambda}'(t)\mathbf{g}(\mathbf{x}, \mathbf{u}; t) \quad (4)$$

where $\mathbf{p}(t) \in \mathbb{R}^n$ is a Lagrange multiplier vector (or co-state) for the dynamic constraint (1) and $\boldsymbol{\lambda}(t) \in \mathbb{R}^2$ are the Lagrange multipliers for the inequality constraint (3). Note that all $\lambda_i(t) \geq 0$. In the usual way [13], adjoining the constraints with multipliers to the performance index J , we have

$$J_A = \int_0^{t_f} [H(\mathbf{x}, \mathbf{u}, \mathbf{p}, \boldsymbol{\lambda}; t) - \mathbf{p}'(t)\dot{\mathbf{x}}(t)]dt. \quad (5)$$

Following the calculus of variations, the first-order necessary conditions for optimality are [13]

$$\dot{\mathbf{x}}(t) = \frac{\partial H}{\partial \mathbf{p}} = \mathbf{A}\mathbf{x}(t) + \mathbf{B}\mathbf{u}(t) + \mathbf{B}_w w(t), \quad \mathbf{x}(0) = \mathbf{x}_0 \quad (6a)$$

$$\dot{\mathbf{p}}(t) = -\frac{\partial H}{\partial \mathbf{x}} = -\mathbf{Q}\mathbf{x}(t) - \mathbf{S}\mathbf{u}(t) - \mathbf{A}'\mathbf{p}(t) + c_{\max}u(t)\boldsymbol{\lambda}_2(t)\mathbf{T}, \quad \mathbf{p}(t_f) = \mathbf{0} \quad (6b)$$

$$0 = \frac{\partial H}{\partial \mathbf{u}} = \mathbf{S}'\mathbf{x}(t) + \mathbf{R}\mathbf{u}(t) + \mathbf{B}'\mathbf{p}(t) + 2u(t)\boldsymbol{\lambda}_1(t) + (2u(t) - c_{\max}\mathbf{T}'\mathbf{x}(t))\boldsymbol{\lambda}_2(t) \quad (6c)$$

$$\mathbf{0} \geq \frac{\partial H}{\partial \boldsymbol{\lambda}} = \mathbf{g}(\mathbf{x}, \mathbf{u}; t). \quad (6d)$$

Equation (6) constitutes a differential-algebraic TPBVP. The following section gives the solution procedure proposed by Harvey *et al.* [15], which is an extension of [14].

2.1 Solution procedure

To solve the necessary conditions (6), the following quadratic program is solved at each time t :

$$\min_{u(t)} \max_{\lambda(t) \geq \mathbf{0}} H(\mathbf{x}, \mathbf{u}, \mathbf{p}, \lambda; t). \quad (7)$$

The unconstrained optimal control is given by the stationarity condition (6c) for $\lambda = \mathbf{0}$.

$$u_{\text{active}}(t) = -R^{-1}(\mathbf{S}'\mathbf{x}(t) + \mathbf{B}'\mathbf{p}(t)). \quad (8)$$

The subscript active is used here to represent the finite-horizon unconstrained optimal control input, not an LQR or LQG feedback controller. Then, using the following saturation function to ensure feasibility,

$$u_{\text{sat}}(t) = \text{sat}(\mathbf{x}, u_{\text{active}}; t) = \begin{cases} u_{\text{active}} & : \quad \mathbf{g}(\mathbf{x}, u_{\text{active}}; t) \leq \mathbf{0} \\ \arg\{g_j(\mathbf{x}, u; t) = 0\} & : \quad g_j(\mathbf{x}, u_{\text{active}}; t) > 0 \end{cases} \quad (9)$$

At times where the active control input is infeasible we saturate $u(t)$ to the constraint boundary, $g_j(\mathbf{x}, u; t) = 0$, and the j th Lagrange multiplier $\lambda_j(t)$ is determined from (6c) such that the Hamiltonian has a saddle point at the constraint boundary. If two or more constraints are violated, we saturate to the most restrictive constraint.

2.2 Saturation function for semi-active damper

For the semi-active damper constraint (3), the saturation function (9) can be implemented numerically as follows [15]:

1. Calculate $\mathbf{g}(\mathbf{x}, u_{\text{active}}; t)$ and the velocity across the actuator $v(t) = \mathbf{T}'\mathbf{x}(t)$.

2. Perform the following checks:

(a) if $\mathbf{g}(\mathbf{x}, u_{\text{active}}; t) \leq \mathbf{0}$, set $u_{\text{sat}}(t) = u_{\text{active}}(t)$, $\lambda_1(t) = 0$, $\lambda_2(t) = 0$, and break;

(b) if $u_{\text{active}}(t) \cdot v(t) < 0$, set $u_{\text{sat}}(t) = 0$, $\lambda_1(t) = 0$,

$$\lambda_2(t) = (\mathbf{S}'\mathbf{x}(t) + \mathbf{B}'\mathbf{p}(t))/(c_{\text{max}}\mathbf{T}'\mathbf{x}(t)), \quad (10)$$

and break;

(c) if $|v(t)| > u_{\text{max}}/c_{\text{max}}$, set $u_{\text{sat}}(t) = u_{\text{max}} \cdot \text{sign}(u_{\text{active}}(t))$ where $\text{sign}(\cdot)$ is the signum function,

$$\lambda_1(t) = -(\mathbf{S}'\mathbf{x}(t) + R u_{\text{sat}}(t) + \mathbf{B}'\mathbf{p}(t))/(2u_{\text{sat}}(t)), \quad (11)$$

$\lambda_2(t) = 0$, and break;

(d) if $v(t) = 0$, set $u(t) = 0$, $\lambda_1(t) = 0$, $\lambda_2(t) = 0$, and break;

(e) otherwise, set $u_{\text{sat}}(t) = c_{\text{max}}\mathbf{T}'\mathbf{x}(t)$, $\lambda_1(t) = 0$,

$$\lambda_2(t) = -(\mathbf{S}'\mathbf{x}(t) + c_{\text{max}}R\mathbf{T}'\mathbf{x}(t) + \mathbf{B}'\mathbf{p}(t))/(c_{\text{max}}\mathbf{T}'\mathbf{x}(t)), \quad (12)$$

and break.

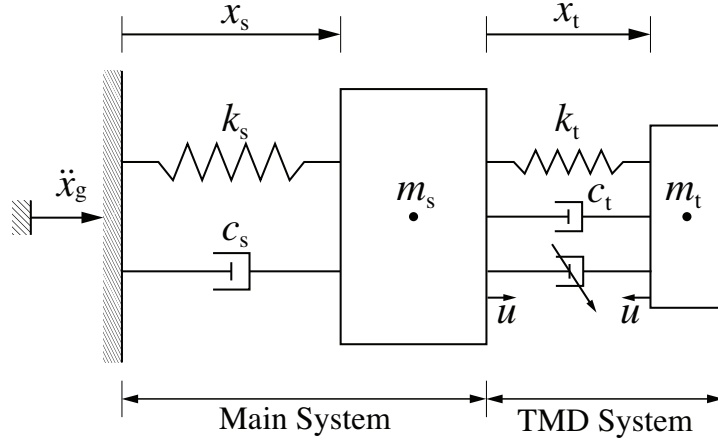


Figure 2: Structural model of a single-degree-of-freedom structure with TMD.

Note that step 2(d) is in place to handle the singularity in (6c) at $v(t) = 0$; i.e., for $v(t) = 0$, the equality constraint $u(t) = 0$ must be satisfied, thus making $\lambda_2(t)$ arbitrary, for which we have chosen $\lambda_2(t) = 0$. In MATLAB, the saturation function can be implemented by calling a function such as `sat(x, uactive, p)` given in Appendix A.

In solving for $u_{\text{sat}}(t)$ and $\lambda(t)$ and substituting them into Equations (6a) and (6b), the TPBVP is now *unconstrained*, as given by

$$\frac{d}{dt} \begin{bmatrix} \mathbf{x}(t) \\ \mathbf{p}(t) \end{bmatrix} = \begin{bmatrix} \mathbf{A} & \mathbf{0} \\ -\mathbf{Q} & -\mathbf{A}' \end{bmatrix} \begin{bmatrix} \mathbf{x}(t) \\ \mathbf{p}(t) \end{bmatrix} + \begin{bmatrix} \mathbf{B} \\ -\mathbf{S} + c_{\max} \lambda_2(t) \mathbf{T} \end{bmatrix} u_{\text{sat}}(t) + \begin{bmatrix} \mathbf{B}_w \\ \mathbf{0} \end{bmatrix} w(t) \quad (13)$$

with boundary conditions

$$\begin{bmatrix} \mathbf{x}(0) \\ \mathbf{p}(t_f) \end{bmatrix} = \begin{bmatrix} \mathbf{x}_0 \\ \mathbf{0} \end{bmatrix}. \quad (14)$$

To ensure that the necessary conditions (6) are satisfied, the states $\mathbf{x}(t)$ and co-states $\mathbf{p}(t)$ must be determined by numerically solving (13). Numerical methods to solve unconstrained TPBVPs are well established, e.g. shooting methods, finite differences, and finite elements. In this study, the unconstrained TPBVP is solved with the MATLAB function `bvp4c.m`, which implements a collocation method with piecewise cubic interpolation satisfying the boundary conditions over each time step [16]. The following section gives a numerical demonstration of how to implement `bvp4c` to solve (13) and determine optimal control trajectories that adhere to semi-active constraints.

3 Numerical Example

3.1 Tuned-mass-damper system

To illustrate the performance optimization of a semi-active system, the semi-active performance of a simple semi-active TMD model is optimized to suppress seismic responses. The model is very similar to the system studied by Hrovat *et al.* [17], except that in this study the system is subjected to base acceleration \ddot{x}_g , as shown in Figure 2. The mass-normalized equations of motion which model the vibration of the system are

$$(1 + \mu)\ddot{x}_s(t) + \mu\ddot{x}_t(t) + 2\zeta_s\omega_s\dot{x}_s(t) + \omega_s^2x_s(t) = -(1 + \mu)\ddot{x}_g(t) \quad (15a)$$

$$\ddot{x}_s(t) + \ddot{x}_t(t) + 2\zeta_t\omega_t\dot{x}_t(t) + \omega_t^2x_t(t) + u(t)/m_t = -\ddot{x}_g(t) \quad (15b)$$

with the following parameters defined [17]:

$$\mu = \frac{m_t}{m_s}, \quad \omega_s = \sqrt{\frac{k_s}{m_s}}, \quad \omega_t = \sqrt{\frac{k_t}{m_t}}, \quad \zeta_s = \frac{c_s}{2m_s\omega_s}, \quad \zeta_t = \frac{c_t}{2m_t\omega_t}. \quad (16)$$

Equation (15) can be represented in state-space form (1) where $\mathbf{x}(t) = [x_s(t), x_t(t), \dot{x}_s(t), \dot{x}_t(t)]' \in \mathbb{R}^4$, $w(t) = \ddot{x}_g(t)$,

$$\mathbf{A} = \begin{bmatrix} 0 & 0 & 1 & 0 \\ 0 & 0 & 0 & 1 \\ -\omega_s^2 & \mu\omega_t^2 & -2\zeta_s\omega_s & \mu 2\zeta_t\omega_t \\ \omega_s^2 & -(1+\mu)\omega_t^2 & 2\zeta_s\omega_s & -(1+\mu)2\zeta_t\omega_t \end{bmatrix}, \quad \mathbf{B} = \begin{bmatrix} 0 \\ 0 \\ \mu/m_t \\ -(1+\mu)/m_t \end{bmatrix}, \quad \mathbf{B}_w = \begin{bmatrix} 0 \\ 0 \\ -1 \\ 0 \end{bmatrix}. \quad (17)$$

The mass ratio $\mu = 0.10$ and the TMD natural frequency ω_t is the optimum tuning frequency ω_t^* discussed in Section 3.1.1. Table 1 gives numerical values for the system parameters. As a benchmark for comparison, the optimal performance will be compared to the following three cases.

3.1.1 Optimized passive TMD

A passive TMD with optimized parameters is used as the first benchmark for comparison. Parameter optimization of the passive TMD results in the following expressions for ω_t^* and ζ_t^* [18]:

$$\text{optimum tuning frequency:} \quad \omega_t^* = \frac{\omega_s}{1+\mu}, \quad (18a)$$

$$\text{optimum passive damping ratio:} \quad \zeta_t^* = \sqrt{\frac{3\mu}{8(1+\mu)}}. \quad (18b)$$

Table 1 gives numerical values for the passive TMD system parameters. Note the passive damping force, $c_t^* \mathbf{T}' \mathbf{x}(t)$, is to be clipped at the same level u_{\max} as the semi-active device to ensure a fair comparison.

3.1.2 Clipped-LQR

The second control scheme – clipped-LQR – is a somewhat *ad hoc* yet prevalent sub-optimal scheme, based on linear quadratic regulator (LQR) theory. Define the linear feedback control $u_{\text{LQR}} = -R^{-1}(\mathbf{P}\mathbf{B} + \mathbf{S})' \mathbf{x}$, where \mathbf{P} is found by solving the algebraic Riccati equation

$$\mathbf{0} = \mathbf{A}'\mathbf{P} + \mathbf{P}\mathbf{A} - (\mathbf{P}\mathbf{B} + \mathbf{S})R^{-1}(\mathbf{P}\mathbf{B} + \mathbf{S})' + \mathbf{Q}. \quad (19)$$

In order to be able to be implemented u_{LQR} directly in the compliant damper model, feedback controls are *clipped* when the prescribed forces is infeasible.

3.1.3 Uncontrolled

Finally, the performance of the optimal control trajectory is juxtaposed against an uncontrolled structure with no TMD, which is essentially the response of a SDOF system with parameters given in the first column of Table 1.

3.2 Pulse-like disturbance model

Two types of ground motions are considered in this study: an idealized pulse and a historical ground motion record. Analytical pulse models are useful in the systematic design and assessment of seismic protective systems. Furthermore, due to the smooth nature of the disturbance and responses, simulations are less computationally expensive, which can accelerate parameter tuning, e.g. determining weighting matrices \mathbf{Q} , \mathbf{R} , and \mathbf{S} .

The pulse acceleration in this study is given by [15]

$$\ddot{x}_g(t) = \left(\frac{t-t_0}{\tau}\right)^\eta \exp\left(-\frac{t-t_0}{\tau}\right) \cos(\omega_p(t-t_0) - \phi). \quad (20)$$

Accelerations are zero for $t < t_0$ and have a predominant period $T_p = 2\pi/\omega_p$. In order for the record to contain N cycles of strong motion, the decay time constant τ is set to $NT_p/4$. Ground acceleration records should have negligibly small velocity and small displacement at the end of the record. For a zero terminal velocity, the phase constant ϕ should be [15]

$$\tan \phi = \frac{3(\tau\omega_p)^2 - 1}{3(\tau\omega_p) - (\tau\omega_p)^3}. \quad (21)$$

To enforce small residual displacements the second derivative of a scaled logistic is iteratively subtracted from the acceleration record until the displacement at the end of the record is close to zero. The associated fixed-point map is

$$\ddot{x}_g(t) \leftarrow \ddot{x}_g(t) - x_g(t_f) e^{-s}(1 + e^{-s})^3(e^{-s} - 1)/(\tau/2)^2, \quad (22)$$

where $x_g(t_f)$ is the displacement at the end of the record, and s is a scaled time variable equal to $(t - t_0 - \eta\tau)/(\tau/2)$. In applying the fixed-point-map of equation (22), accelerations should not be re-set to zero for $t < t_0$. For $\eta = 2$, $1 < N < 5$, and $0.5 < T_p < 4$ s, peak velocities scale with T_p and are approximately given by

$$\dot{x}_g^{\max} = \max \left[4.063N^{-2.165}e^{-4.403/N}, 2.329N^{-1.336}e^{-5.693/N} \right] T_p \pm 0.5\%. \quad (23)$$

He and Agrawal [19] validated a similar pulse model through comparison with numerous ground motions, corresponding response spectra, and the performance of passive energy dissipation systems. The pulse model used in the present work has a terminal velocity of zero (from equation (21)) and a terminal displacement of zero (from equation (22)). In this study, disturbance waveforms were scaled to match prescribed peak velocity values V_p by scaling accelerations by a factor of V_p/\dot{x}_g^{\max} . Figure 3(a) illustrates a sample disturbance record using the following disturbance parameters: $\omega_p = 1.0$ rad/s, $V_p = 0.8$ m/s, $t_0 = 2.0$ s, $\eta = 2$, and $N = 2.0$.

3.3 Performance index and numerical values

In this example the Lagrangian $L(\cdot)$ is selected as the square of the total acceleration of the primary structure:

$$L(\mathbf{x}, u; t) = \frac{1}{2} [\ddot{x}_g(t) + \ddot{x}_s(t)]^2 \equiv \frac{1}{2} [\mathbf{A}_{(3,\cdot)}\mathbf{x}(t) + \mathbf{B}_{(3)}u(t)]^2 \quad (24)$$

where $\mathbf{A}_{(3,\cdot)}$ is the third row of the dynamics matrix and $\mathbf{B}_{(3)}$ is the third entry of the control input vector. The state, control input, and cross weighting matrices are thus $\mathbf{Q} = \mathbf{A}'_{(3,\cdot)}\mathbf{A}_{(3,\cdot)}$, $\mathbf{R} = \mathbf{B}_{(3)}\mathbf{B}_{(3)}$, and $\mathbf{S} = \mathbf{A}'_{(3,\cdot)}\mathbf{B}_{(3)}$.

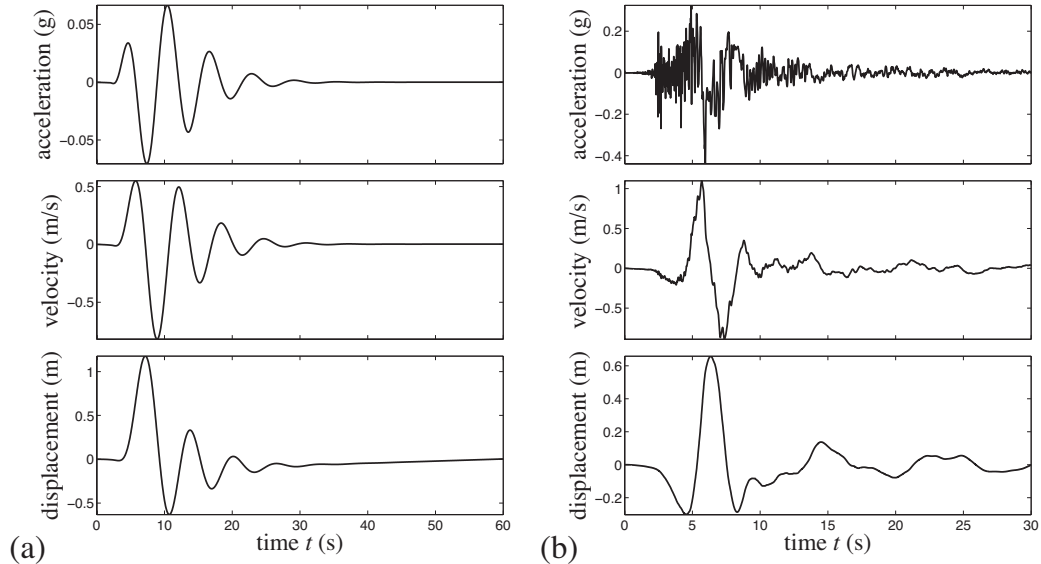


Figure 3: Acceleration, velocity, and displacement time histories of a pulse-like ground motion and a recorded ground motion. (a) Pulse-like ground motion for parameter values given in Section 3.2; (b) 1979 Imperial Valley earthquake, El Centro Array #6 -230°.

We consider only adjustable control forces $u(t)$ that are constrained by (3). For the constraint $g_1(\mathbf{x}, u; t)$, the maximum semi-active force $u_{\max} = 5 \times 10^4$ N is used in simulation. For the maximum dissipating constraint $g_2(\mathbf{x}, u; t)$, the velocity across the actuator is $\dot{x}_t = \mathbf{T}'\mathbf{x}$ for which $\mathbf{T}' = [0 \ 0 \ 0 \ 1]$. The maximum damping coefficient is taken to be $c_{\max} = 2\zeta_{\max}\omega_t m_t$, with $\zeta_{\max} = 18$ percent.

3.4 MATLAB procedure

Appendix A gives sample code for this example. The procedure involves first initializing the model parameters (line 2). The variables dt and nT are the time step and length of the time vector \mathbf{t} , respectively, used to linearly interpolate the disturbance history w at intermediate times. The initial states \mathbf{x}_0 and terminal co-states \mathbf{p}_f must also be specified. Concatenating the state and co-state into a single vector, define $\mathbf{z} = [\mathbf{x}; \mathbf{p}]$. Specify global variables (line 1), which are accessed by the ODE function $\mathbf{zdot}(\mathbf{t}, \mathbf{z}, w)$, the boundary condition (BC) function $\mathbf{bcfun}(\mathbf{z}_0, \mathbf{z}_f, \mathbf{x}_0, \mathbf{p}_f)$, and the saturation function $\text{sat}(\mathbf{x}, u_{\text{active}}, p)$.

In line 4, the options are specified using `bvpset`. The maximum mesh discretization (the maximum number of time steps) `NMax` is increased to avoid premature termination of `bvp4c`; because `bvp4c` uses an adaptive mesh, with `NMax` too small the evaluation may be terminated before convergence is met. By setting `Stats` to `on`, the simulation results are displayed, e.g. number of ODE calls, number of BC calls.

`bvp4c` requires an initial guess for the trajectories, for which a constant initialization of $5 \times \text{eps}$ is selected for this example using the function `bvpinit`. An initial guess of zero is not permitted because the BCs would be automatically satisfied and `bvp4c` would fail to run.

In line 6, `bvp4c` is called. The four arguments to `bvp4c` are the ODE function $\mathbf{zdot}(\mathbf{t}, \mathbf{z}, w)$ given in Appendix A which represents (13); the BC function (14), given in Appendix A by the function $\mathbf{bcfun}(\mathbf{z}_0, \mathbf{z}_f, \mathbf{x}_0, \mathbf{p}_f)$; the initial guess for the solution `solinit`; and the previously defined options. The output `sol` of `bvp4c` must then be evaluated using the command $\mathbf{z} = \text{deval}(\text{sol}, \mathbf{t})$ for the time series \mathbf{t} . Finally, the state and co-state histories may be extracted from \mathbf{z} .

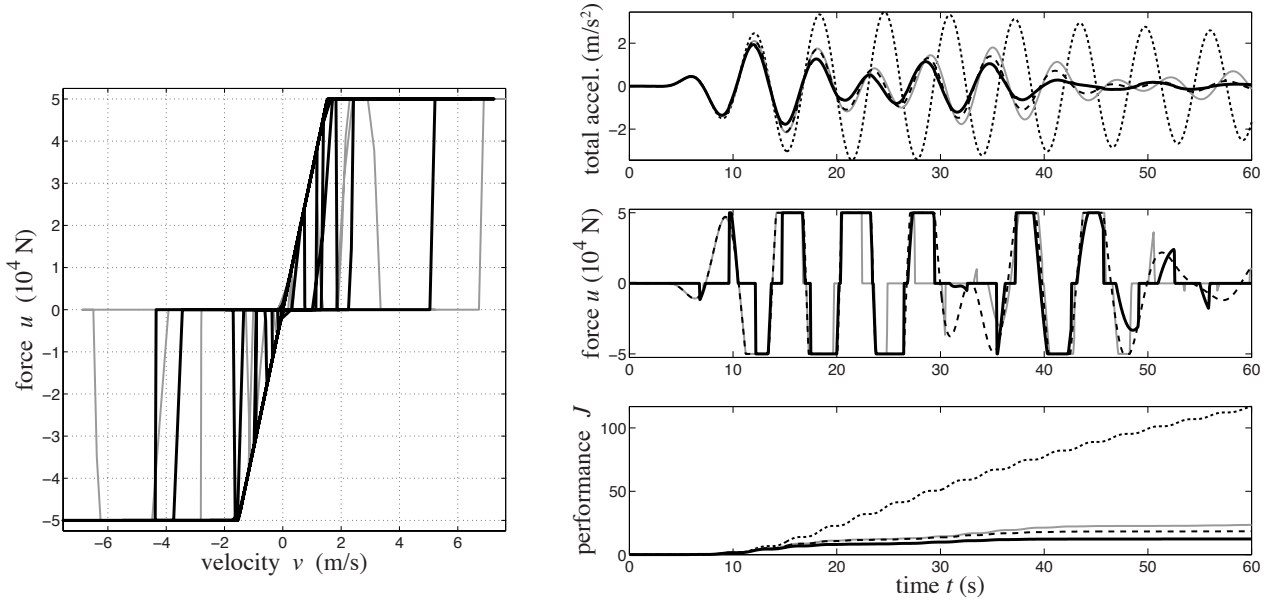


Figure 4: Responses to a pulse-like disturbance: comparison of optimal (thick) with passive (dashed), clipped-LQR (gray), and uncontrolled (dotted).

3.5 Optimized semi-active control trajectories

The proposed method is now applied to the previously described TMD model under two loading scenarios. First, a pulse-like disturbance is used to validate that the optimized trajectories satisfy the necessary conditions. Then, optimal semi-active trajectories are computed for a recorded earthquake ground motion. In both cases, a comparison is made between the optimal semi-active controller, the optimized passive TMD, the clipped-LQR controller, and the uncontrolled system.

3.5.1 Pulse-like ground motion

The converged optimal semi-active trajectory, the passive trajectory, the clipped-LQR trajectory, and uncontrolled trajectory are given in Figure 4, along with the primary structure total acceleration ($\ddot{x}_g + \ddot{x}_s$) history and the performance J history. The control force $u(t)$ versus the velocity across the actuator $v(t)$ shows that the semi-active constraint is strictly satisfied. As evident from the control force history, the optimal trajectory is ‘on’ less than the clipped-LQR and passive controllers (in an L_1 sense). As observed from Figure 4, the optimal control reduces significantly the mean-square acceleration (i.e. J), as compared to the passive, clipped-LQR, and uncontrolled systems—approximately 33%, 47%, and 89%, respectively.

Figure 5 shows the constraint time histories and the corresponding Lagrange multiplier. We see that the complementary slackness condition

$$\lambda_i(t) \begin{cases} = 0 & : \quad g_i(\mathbf{x}, u; t) < 0 \\ \geq 0 & : \quad g_i(\mathbf{x}, u; t) = 0 \end{cases} \quad (25)$$

is strictly satisfied by the optimal trajectory. That is to say, the Lagrange multiplier is turned on when the control input desires to be infeasible, pinning the trajectory to the constraint boundary. It is clear to see that the term $\lambda'(t)g(\mathbf{x}, u; t) \equiv 0, \forall t$.

Figure 6 shows converged control histories from three initial guesses: constant at $5 \cdot \text{eps} \cdot \text{ones}(8, 1)$, constant at $10 \cdot \text{ones}(8, 1)$, and the active solution. The number of ODE calls to reach convergence

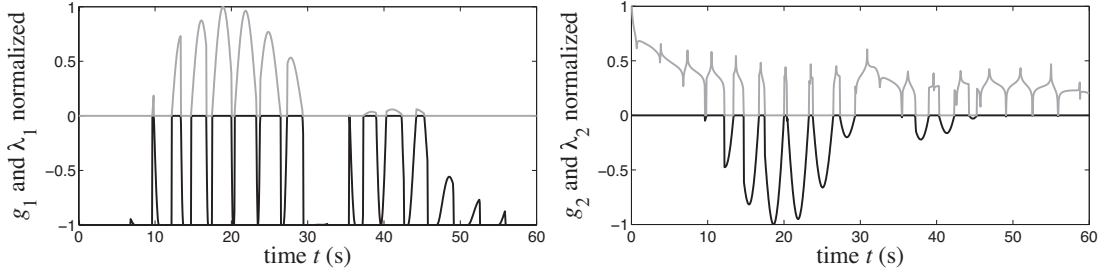


Figure 5: Normalized constraint $g_i(\mathbf{x}, u; t)$ and normalized Lagrange multiplier $\lambda_i(t)$ time histories (black: constraint $g_i(\mathbf{x}, u; t)$; gray: Lagrange multiplier $\lambda_i(t)$).

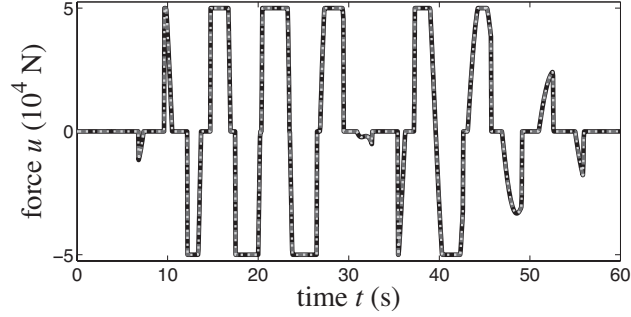


Figure 6: Converged control force histories from three initial guesses (black: $5 \times \text{eps}$; dashed dark gray: 10; dotted light gray: active solution).

varies: approximately 5.4×10^5 , 3.6×10^5 , and 5.5×10^5 ODE calls, respectively. The speed of convergence is dependent on the initial guess; with a bad initial guess convergence may be very slow. Nonetheless, for all three initial guesses, the method converges to the same optimal trajectories.

3.5.2 Earthquake ground motion

Now we consider a recorded earthquake ground motion. The recorded ground motion is the E06230 component of the 1979 Imperial Valley earthquake [20]. Figure 3(b) illustrates the disturbance record. The optimal control force trajectory is illustrated in Figure 7, along with the structure’s total acceleration and the performance history. Once again, the optimal control significantly outperforms the uncontrolled system (68%) and marginally outperforms the passive and clipped-LQR controllers (15% and 21%, respectively). The proposed method is robust enough to handle non-smooth ground motions such as recorded earthquake records. However, convergence required approximately 1.4×10^6 ODE evaluations.

4 Conclusions

The answer to the question “How much could semi-active control improve performance in this application?” can be powerful in establishing the potential for a new semi-active control device or a new semi-active control application. Methods of constrained optimal control, as outlined in this short tutorial paper, provide an easy and ready means to generate such answers. The illustrative example presented is meant to serve as a guide and is therefore intentionally simple.

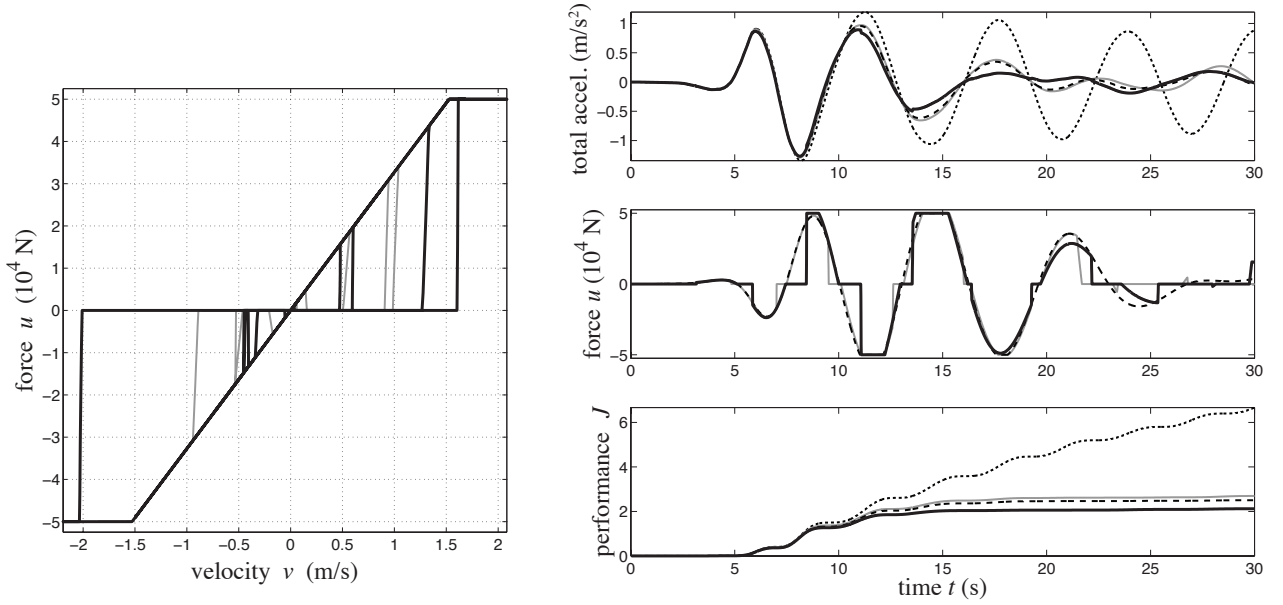


Figure 7: Recorded ground motion test: comparison of optimal (thick) with passive (dashed), clipped-LQR (gray), and uncontrolled (dotted).

5 Future work

Logical extensions to this work are numerous and should be pursued. For example:

- The statistical optimal performance of the controlled system to large earthquake data sets would show the potential of semi-active control in variance reduction.
- Incorporating time-lag into the semi-active damper, where the semi-active damping force is given by $\dot{f}(t) = (f(t) - u(t))/T$ and T is the time-lag, typically 0.02 to 0.10 seconds, would add realism to the simulation results. The state equations would remain linear.
- Adding dynamics to the semi-active damping model would add further realism to the study. For example, a Maxwell viscoelastic element with a controllable damping term is modeled as

$$\dot{f}(t) = k[v(t) - f(t)/(c_{\max}u(t) + c_o)]$$

and the constraint is $u(t)(u(t) - 1) \leq 0$. Although such a system has non-linear state and co-state dynamics, the boundary value problem solution described here applies equally well.

- Other non-linear semi-active device models (e.g. MR dampers, pneumatic springs) could be assessed.
- The effect of inelastic structural behavior on optimal semi-active performance could be assessed.
- Systems with multiple control devices may be studied. In doing so, care must be taken in the saturation function so that coupling between devices is properly accounted for.
- In earthquake engineering, peak responses are typically of greater interest than mean squared responses [20]. Extending this method to suppress peak response is a matter of removing the quadratic state cost, so that

$$J = \int_0^{t_f} \frac{1}{2} R u^2(t) dt,$$

and adding a constraint on the peak response, for example,

$$g_x = \max |x_s(t)| - x_{\text{allow}} \leq 0.$$

The method here would be to iteratively reduce x_{allow} until no feasible solution can be found.

- The methodology presented in this paper can be extended to minimizing peak responses by changing the quadratic integrand to a fourth or higher (even) order, and by reducing the time horizon to the first few large cycles of response. Doing so would result in non-linear co-state dynamics.
- A set of Pareto-optimal solutions, parameterized, for example, by the ratio α weighting total acceleration and displacement, e.g.

$$J = \frac{1}{2} \int_0^{t_f} [\alpha(\ddot{x}_g + \ddot{x}_s)^2 + (1 - \alpha)x_s^2] dt,$$

would provide a set of solutions from which the most desirable solution can be selected.

- Optimal control trajectories could be investigated and parameterized in order to develop a class of non-linear feedback control rules inspired by these optimal performance studies.

Acknowledgements

This material is based upon work supported by the National Science Foundation under grant No. NSF-CMMI-0900324. Any opinions, findings, and conclusions or recommendations expressed in this material are those of the authors and do not necessarily reflect the views of the National Science Foundation.

A MATLAB functions

The full MATLAB code used to generate the figures in this paper may be found at <http://www.duke.edu/~hpgavin/osc>. The essentials are given below.

Sample code to run `bvp4c.m`:

```

1 global A B Bw Q R S T umax cmax dt nT n
2 % initialize parameters: A, B, Bw <- eq'n (17); w, t <- eq'ns (20-23); and
3 %   Q, R, S, T, umax, cmax <- Section 3.3
4 nT = length(t); dt = t(2)-t(1)% length and time step of disturbance record
5 x0 = zeros(n,1); pf = zeros(n,1); % initial states and terminal co-states
6 options = bvpset('NMax',20*nT,'Stats','on'); % set options
7 solinit = bvpinit(t,5*eps*ones(2*n,1)); % initialize solution
8 sol = bvp4c(@(t,z) zdot(t,z,w), @(z0,zf) bcfun(z0,zf,x0,pf,n),solinit,options);
9 z = deval(sol,t); x = z(1:n,:); p = z(n+1:2*n,:); % extract states and co-states

```

Unconstrained BVP function:

```

1 function zdot = zdot(t,z,w)
2 global A B Bw Q R S T cmax dt nT n
3 i = min(nT-1,floor(t/dt)+1); % the current time step
4 wi = w(i) + (w(i+1)-w(i))/dt*(t - (i-1)*dt); % interpolate disturbance
5 x = z(1:n); p = z(n+1:2*n); % state and co-state vectors
6 uactive = -R\'(S\'*x + B\'*p); % unconstrained optimal control

```

```

7 [usat,lambda] = sat(x,uactive,p); % saturated controls and Lagrange multipliers
8 % BVP equations for states and co-states ...
9 zdot = [ A*x          + B*usat + Bw*wi
10        -Q*x - A'*p - S*usat + lambda(2)*cmax*T*usat ];

```

Boundary condition (BC) function:

```

1 function bc = bcfun(z0,zf,x0,pf,n)
2 bc = [ z0(1:n,1)-x0 ; zf(n+1:2*n,end)-pf ];

```

Saturation function:

```

1 function [usat,lambda] = sat(x,uactive,p)
2 global umax cmax B R S T
3 g = [ uactive^2 - umax^2 ; uactive*(uactive - cmax*T'*x) ]; % constraints
4 v = T'*x; % velocity across semi-active damper
5 if g(1) <= 0 && g(2) <= 0
6     usat = uactive; lambda = [ 0 ; 0 ]; return
7 elseif uactive*v < 0
8     usat = 0; lambda = [ 0 ; -(S'*x+R*usat+B'*p)/(2*usat-cmax*v) ]; return
9 elseif abs(v) > umax/cmax
10    usat = umax*sign(v); lambda = [ -(S'*x+R*usat+B'*p)/(2*usat) ; 0 ]; return
11 elseif v == 0
12    usat = 0; lambda = [ 0 ; 0 ]; return
13 else
14    usat = cmax*v; lambda = [ 0 ; -(R*usat+S'*x+B'*p)/(2*usat-cmax*v) ]; return
15 end

```

References

- [1] Housner GW, Bergman LA, Caughey TK, Chassiakos AG, Claus RO, Masri SF, Skelton RE, Soong TT, Spencer BF, Yao JTP. Structural control: Past, present, and future. *Journal of Engineering Mechanics* 1997; **123**:897–971.
- [2] Symans MD, Constantinou MC. Semi-active control systems for seismic protection of structures: a state- of-the-art review. *Engineering Structures* 1999; **21**:469–487.
- [3] Nagarajaiah S. Adaptive passive, semiactive, smart tuned mass dampers: identification and control using empirical mode decomposition, hilbert transform, and short-term fourier transform. *Structural Control and Health Monitoring* 2009; **16**:800–841.
- [4] Kang J, Kim HS, Lee DG. Mitigation of wind response of a tall building using semi-active tuned mass dampers. *Structural Design of Tall and Special Buildings* 2011; **20**:552–565.
- [5] Ledezma-Ramirez DF, Ferguson NS, Brennan MJ. Shock isolation using an isolator with switchable stiffness. *Journal of Sound and Vibration* 2011; **330**:868–882.
- [6] Pasala DTR, Nagarajaiah S, Grigoriadis KM. Tracking control of variable stiffness hysteretic-systems using linear-parameter-varying gain-scheduled controller. *Smart Structures and Systems* 2012; **9**:373–392.
- [7] Rodgers GW, Chase JG, Roland T, MacRae GA. Spectral analysis for a semi-active-passive net-zero base-shear design concept. *Earthquake Engineering and Structural Dynamics* 2012; **41**:1207–1216.

- [8] Cassidy IL, Scruggs JT, Behrens S, Gavin HP. Design and experimental characterization of an electromagnetic transducer for large-scale vibratory energy harvesting applications. *Journal of Intelligent Material Systems and Structures* 2011; **22**:2009–2024.
- [9] Chen C, Liao WH. A self-sensing magnetorheological damper with power generation. *Smart Materials and Structures* 2012; **21**:025 041.
- [10] Jiang Z, Christenson RE. A fully dynamic magneto-rheological fluid damper model. *Smart Materials and Structures* 2012; **21**:065 002.
- [11] Laflamme S, Taylor D, Maane MA, Connor JJ. Modified friction device for control of large-scale systems. *Structural Control and Health Monitoring* 2012; **19**:548–564.
- [12] Lin GL, Lin CC, Lu LY, Ho YB. Experimental verification of seismic vibration control using a semi-active friction tuned mass damper. *Earthquake Engineering and Structural Dynamics* 2012; **41**:813–830.
- [13] Kirk DE. *Optimal Control Theory, An Introduction*. Prentice Hall, 1970.
- [14] Tseng HE, Hedrick JK. Semi-active control laws optimal and sub-optimal. *Vehicle System Dynamics* 1994; **23**:545–569.
- [15] Harvey Jr PS, Gavin HP, Scruggs JT. Optimal performance of constrained control systems. *Smart Materials and Structures* 2012; **21**:085 001.
- [16] Kierzenka J, Shampine LF. A BVP solver based on residual control and the MATLAB PSE. *ACM Transactions on Mathematical Software* 2001; **27**(3):299–316, doi:10.1145/502800.502801.
- [17] Hrovat D, Barak F, Rabins M. Semi-active versus passive or active tuned mass dampers for structural control. *Journal of Engineering Mechanics* 1983; **109**(9):691–705.
- [18] Den Hartog JP. *Mechanical Vibration*. Dover, 1985.
- [19] He WL, Agrawal AK. Analytical model of ground motion pulses for the design and assessment of seismic protective systems. *Journal of Structural Engineering* 2008; **134**:1177–1188.
- [20] Applied Technology Council. Quantification of building seismic performance factors. URL <https://www.atcouncil.org/Projects/atc-63-project.html>.

Building data	Semi-Active TMD data	Passive TMD data [18]
$m_s = 1 \times 10^6$ kg	$m_t = 1 \times 10^5$ kg	$m_t = 1 \times 10^5$ kg
$k_s = 1 \times 10^6$ N/m	$k_t^* = 8.26 \times 10^4$ N/m	$k_t^* = 8.26 \times 10^4$ N/m
$c_s = 2 \times 10^4$ N s/m	$c_t = 1.82 \times 10^3$ N s/m	$c_t^* = 3.36 \times 10^4$ N s/m
$\zeta_s = 0.01$	$\zeta_t = 0.01$	$\zeta_t^* = 0.185$
$\omega_s = 1.0$ rad/s	$\omega_t^* = 0.909$ rad/s	$\omega_t^* = 0.909$ rad/s

Table 1: Parameter values used in simulation.